Electrochimica Acta 124 (2014) 150–155

Contents lists available at ScienceDirect

Electrochimica Acta

journal homepage: www.elsevier.com/locate/electacta

Localized corrosion evaluation of the ASTM F139 stainless steel marked by laser using scanning vibrating electrode technique, X-ray photoelectron spectroscopy and Mott–Schottky techniques

Eurico F. Pieretti[a,*], Sara M. Manhabosco[b], Luís F.P. Dick[b,**,1], Steve Hinder[c], Isolda Costa[a,***]

[a] Instituto de Pesquisas Energéticas e Nucleares (IPEN/CNEN), Av. Prof. Lineu Prestes 2242, 05422.970 São Paulo, SP, Brazil
[b] Lab. de Processos Eletroquímicos e Corrosão, Universidade Federal do Rio Grande do Sul, Av. Bento Gonçalves 9500, 91501.970 Porto Alegre, Brazil
[c] Faculty of Engineering and Physical Sciences, University of Surrey, Guildford, UK

ARTICLE INFO

Article history:
Received 15 April 2013
Received in revised form 11 October 2013
Accepted 19 October 2013
Available online 1 November 2013

Keywords:
Localized Corrosion
ASTM F139
Biomaterials
SVET
XPS
Mott–Schottky

ABSTRACT

The effect of laser engraving on the corrosion resistance of ASTM F139 stainless steel (SS) has been investigated by electrochemical techniques. The nucleation of localized corrosion on this biomaterial was evaluated by scanning vibrating electrode technique (SVET) in a phosphate buffered saline solution (PBS) of pH 7.4. The Mott–Schottky approach was used to determine the electronic properties of the passive film, also chemically characterized by X-ray photoelectron spectroscopy (XPS). SVET allowed the identification of the anodic zones on the surface of the SS marked by laser technique that were associated with the heat-affected areas. Metallic drops solidified on the laser marked surface dissolved actively at OCP and favoured the nucleation of crevice corrosion, while at the pitting potential, pits nucleate preferentially on the laser marks. XPS results showed that laser engraving caused large chemical modification of the surface. Mott–Schottky results indicated a more defective oxide layer with a larger number of donors on the laser marked surface comparatively to that without marks.

1. Introduction

The metallic materials used in implants or prostheses are generally passive materials and therefore are subject to localized corrosion, when in contact with body fluids that contain chloride ions. One of the most common types of corrosion observed on metallic implants is pitting [1]. The production processes involved in implants manufacturing also affect their corrosion resistance, specifically those that influence the surface finishing. The final stage of implant devices production consists in marking the surface for identification and traceability of the manufactured material. Among the marking techniques, the laser type is mainly adopted due to its inherent characteristics, such as high rate and reproducibility. Previously a deleterious influence of laser shock processing (LSP) on the corrosion behaviour of the 2050-T8 aluminium alloy has been observed [2]. In the present study, the influence of laser marking for implant identification on the corrosion resistance of the ASTM F139 stainless steel has been investigated by electrochemical techniques. This stainless steel which is used for surgical implants is a low-carbon version of the AISI 316, vacuum arc remelted to reduce impurities.

According to Gittens et al. [3] even small currents produced during corrosion of an implant could have a negative impact on the surrounding tissue and cause the rejection of the implant. In order to evaluate the effect of the laser beam marking on the material corrosion resistance, the scanning vibrating electrode technique (SVET) was used in this study. Many authors [4–8] used the SVET technique as a tool for galvanic or localized corrosion studies. However, in most published studies, the tested samples were specially prepared using dissimilar metals to form galvanic couples of well-known behaviour [7,8]. In this work, SVET was used to detect the initial stages of pit nucleation and the possible formation of cathodic and anodic elements due to the laser marking of the surface used for identification of stainless steel prosthesis. Additionally, the composition of passive films on the marked areas was characterized by XPS and their electronic conductivity properties, evaluated by the Mott–Schottky approach. The model of double

* Corresponding author. Tel.:+55 1131339226.
** Corresponding author.
*** Corresponding author.
E-mail addresses: efpieretti@usp.br, e_pieretti@terra.com.br (E.F. Pieretti), lfdick@ufrgs.br (L.F.P. Dick), s.hinder@surrey.ac.uk (S. Hinder), icosta@ipen.br (I. Costa).
[1] ISE Member.

0013-4686/$ – see front matter © 2013 Elsevier Ltd. All rights reserved.
http://dx.doi.org/10.1016/j.electacta.2013.10.137

layer of oxides formed on austenitic stainless steels [9–16] proposes a behaviour of an n-type semiconductor in the outer layer next to the solution, and a p-type behaviour in the inner layer, closer to the substrate. X-ray photoelectron spectroscopy (XPS) is a technique often used to characterize thin passive films formed on stainless steels [17,18].

2. Experimental

Samples of the stainless steel ASTM F139, with the composition (wt.%): 0.38 Si, 2.09 Mn, 0.026 P, 2.59 Mo, 18.32 Cr, 14.33 Ni, 0.023 C, 0.0003 S, and Fe balance, were marked by laser. Laser marking was carried out using a pulsed Nd:YAG laser, at wavelength of 1064 nm, with 20 Hz of frequency and a scanning speed of 4 mm s^{-1}. The marking procedure consisted of recording a sequence of the numeral 8 (eight), on the surface in order to cover a large proportion of the areas exposed to the electrolyte. The marking process of the numeral "8" causes the overlapping of the laser (it passes twice at the same area) at the centre of the marked "8". The electrochemical experiments were carried out at 25 °C in an aerated phosphate buffered saline (PBS) containing NaCl 8.8 g/L, KCl 0.2 g/L, Na_2HPO_4 1.15 g/L, KH_2PO_4 0.2 g/L, with a pH value of 7.4 and a conductivity of 15.35 mS. Current density maps were acquired on this biomaterial using an Applicable Electronics SVET assembly. This technique measures ohmic drops in the electrolyte above the sample surface and converts it to local current densities based on the Ohm's law and the value of the conductivity of the solution [6]. The vibrating microelectrode had a spherical platinum black tip of ∅ = 10 μm and vibrated at the distance of 100 μm above the sample surface with an amplitude of 10 μm, limiting the lateral resolution of acquired *i*-maps to approximately 20 μm. This is much smaller than the width of the laser mark on samples surface, which ranges from 160 to 300 μm. An auxiliary microelectrode, similar to the vibrating microelectrode, was used during electrode vibration as a reference, for the measurement of the mentioned ohmic drops associated to the current flow. The counter electrode was a 250 μm Pt wire placed in the PBS solution. The reference electrode in the SVET system was an Ag wire previously anodized in 0.14 mol/L KCl and placed directly in the PBS solution, which contains 0.1396 mol/L of chloride ions. The potential referred in the text were converted to the 3 M Cl^- AgCl/Ag electrode ($E_{AgCl/Ag}$, 3 M = 210 mV SHE). The samples for the SVET measurements were embedded under vacuum in epoxy to minimize crevice corrosion. For cyclic voltammetry (CV) tests, a commercial AgCl/Ag electrode, immersed in 3 mol/L KCl solution was used.

The electronic properties of passive film were determined by employing the Mott–Schottky approach, using a Gamry PCI4/300 equipment. The capacitance measurements were performed at a frequency of 1 kHz. Polarization was applied at successive steps of 50 mV in the negative direction from 500 mV to −1000 mV ($E_{AgCl/Ag}$). The Mott–Schottky results were reported as the inverse square of an apparent interfacial capacitance *C* as function of potential *E*, with: $C = -1/2\pi fZ''$, where *f* is the test frequency and *Z*" is the imaginary component of the interfacial impedance [9,10]; the interface passive film/electrolyte is described by the expression [11–13]:

$$\frac{1}{C^2} = \frac{2}{\varepsilon\varepsilon_0 q N_q}\left(E_{FB} - E + \frac{kT}{e}\right)$$

where *C* is the apparent capacitance of the film|electrolyte interface, *E*, the applied potential, ε, the dielectric constant of the passive film, ε_0 the vacuum permittivity, N_q, the density of electron donors or acceptors for doping an n-type or p-type semiconductor, respectively, *q*, the elementary charge, *k*, the Boltzmann constant, *T*, the absolute temperature and E_{FB}, the flat-band potential. For stainless steels, it is often assumed that the semiconducting behaviour

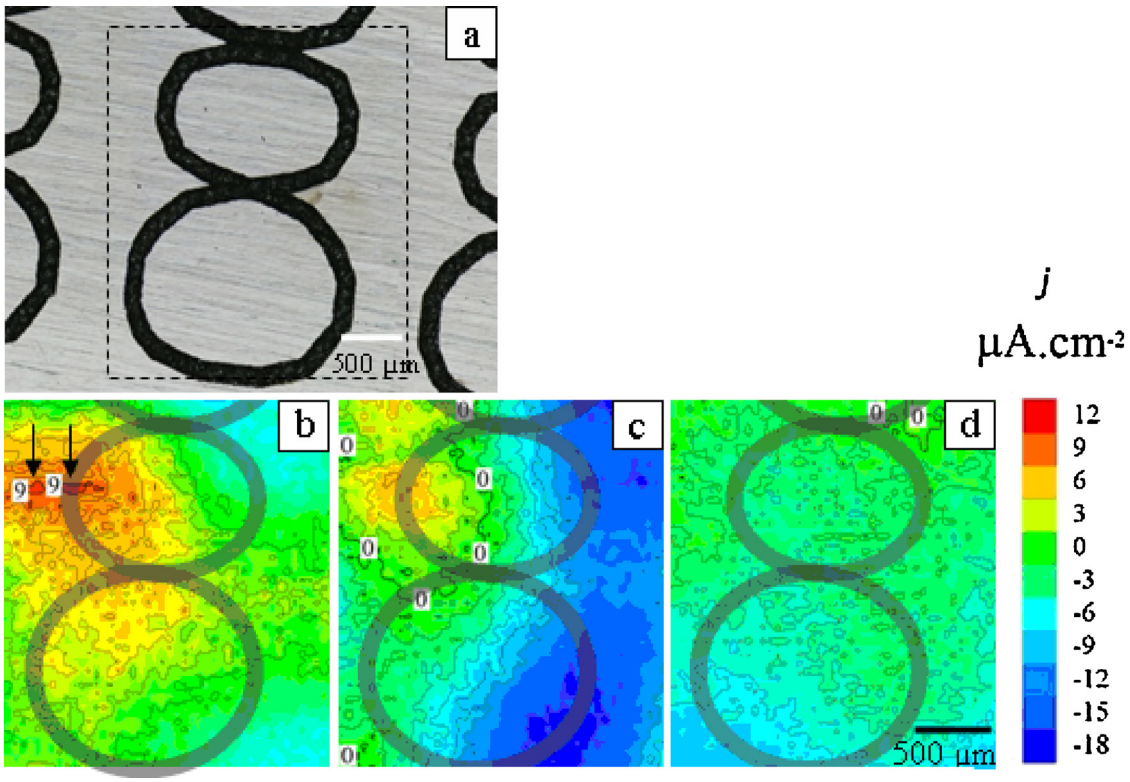

Fig. 1. (a) Optical microscope view of laser marked area where *i*-maps were sequentially acquired in PBS solution by SVET. The measuring window of 2430 × 2140 μm is indicated by the dashed line, (b) *i*-map measured immediately after immersion in PBS (the arrows indicate two anodic spots with *i* = with 9 μA/cm^2), (c) *i*-map after 1 h and (d) after 4 h.

reflects the duplex character of their oxide films, essentially consisting of a mixed spinel oxide of the $(Fe,Ni)_2CrO_4$ type, richer in Cr in the inner region and richer in Fe in the outer one [10]. The positive slope of the C^{2-} *versus E* plot reveals an n-type semiconductor behaviour that is characteristic of a Fe^{2+}-rich spinel; the negative slope, in the other hand, results from the electrochemical behaviour of a p-type semiconductor, related to the presence of Cr^{3+}-rich oxide [10,11]. X-ray photoelectron spectroscopy (XPS) spectra were acquired in a Kratos XSAM HS equipment under ultra-high vacuum ($p \approx 3 \times 10^{-8}$ Torr). The exciter source was magnesium Kα, with energy of 1.2536 keV [14]. For peaks fitting the Shirley method and least squares routine were used [15].

3. Results and discussion

The corrosion mechanism of ASTM F139 marked by laser was evaluated by SVET. Initially, it was repeatedly observed that when a window with *Scotch Tape* was provided on the sample surface to limit the exposed area with a single "8" mark, crevice corrosion always took place at the open circuit potential (OCP), just a few minutes after exposure to the electrolyte at the experimental conditions (25 °C, OCP, NaCl 8.0 g/L + KCl 0.2 g/L), either the surface was laser marked or not (results not shown). No delimitation windows were used in the following SVET-experiments to avoid crevice corrosion. In these cases, *i*-maps were acquired on a fraction of the total exposed area, to avoid measuring currents due to eventual crevice corrosion between the epoxy embedment and the sample border.

Fig. 1 shows *i*-maps of the local ionic currents in the PBS solution obtained on a laser marked sample, when no delimitation window was used, at the OCP. Current maps where repeatedly acquired on the same region with a surface area of 2430 × 2140 μm, which is smaller than the total exposed area, as indicated by the dashed black rectangle in Fig. 1a containing only one "8" laser mark to increase the lateral resolution by observing only a restricted window. Fig. 1b shows the corresponding *i*-map measured immediately after immersion in PBS. It was observed in the example of Fig. 1 and also on other samples that, initially, anodic currents around 10 μA/cm² are observed on some random spots on the laser marked regions, or close to it, which may repassivate after some time. Specifically for the measuring window of Fig. 1a, two anodic spots are seen after immersion, indicated by arrows in Fig. 1b, for *t* = zero h that repassivated after 1 h (Fig. 1c). After some exposure time, cathodic and anodic currents decay continuously to zero, as shown in Fig. 1(c) for 1 h and in Fig. 1(d), for 4 h exposure time. This means that the laser-marked areas contain some highly defective regions that dissolve actively at the open circuit potential in the phosphate buffered saline, but repassivate at OCP, not leading to the nucleation of pits. In fact, several small metal droplets with diameters ranging from 6 to 10 μm are deposited during engraving on the laser mark and surrounding surfaces due to the sudden fusion and partial metal vaporization (Fig. 2a). This may explain the range of measured OCP values after immersion in the PBS solution (OCP = −88 ± 203 mV, $E_{AgCl/Ag}$), as well as the rapid OCP deviations to more active potentials, followed by a slow repassivation of the surface, only observed for laser marked surfaces, as in the example of Fig. 3.

Fig. 2a shows a SEM image of pits related to the laser marked surface, after a cyclic voltammetry test indicated in Fig. 2b. It is clearly seen that a higher pitting susceptibility is associated to the laser marked samples, showing a pitting potential much lower comparatively to the surface without marks, and that the pits are more prone to nucleate on the areas where the laser passed twice, as Fig. 2a illustrates.

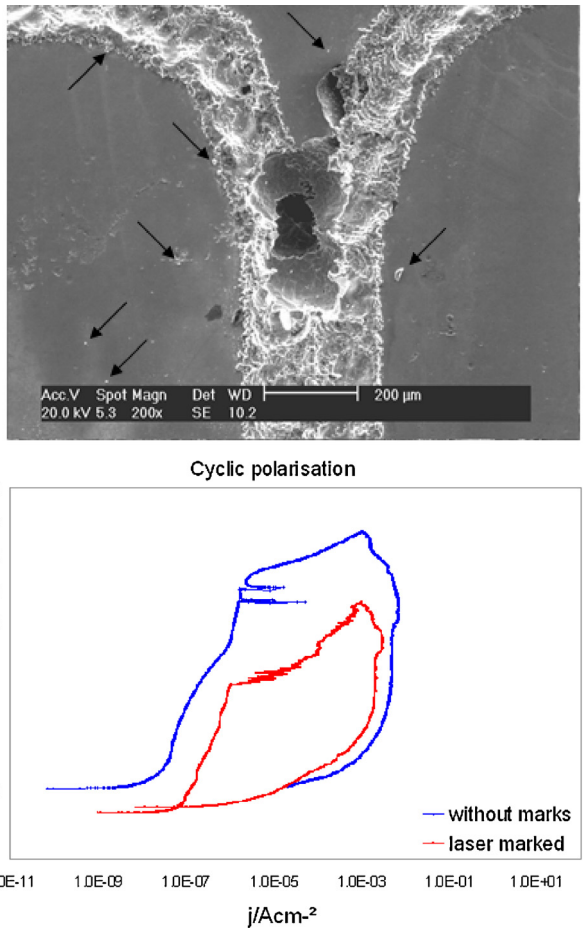

Fig. 2. (a) SEM view (secondary electrons imaging) of pits found at the centred marked area, where the laser beam passes twice. The picture was taken after polarization with 0.1 mV/s up to the pitting potential of +610 mV ($E_{AgCl/Ag}$). The arrows indicate some metal droplets around the laser engraving. (b) Voltamogramm corresponding to (a).

However, if a crevice is present, as the one formed by a delimitation window, then, crevice corrosion is immediately nucleated on areas with laser marks at the OCP with *i* generally 50% higher, comparatively to blank surfaces (not shown). A crevice could be possibly formed between the implant surface and the bone tissue or even a fixation screw. As small corrosion currents could result in implant rejection [3], an artificial crevice was produced simply by embedding the sample cross-section in epoxy (Fig. 4) and this experimental condition was analyzed by acquiring *i*-maps at OCP

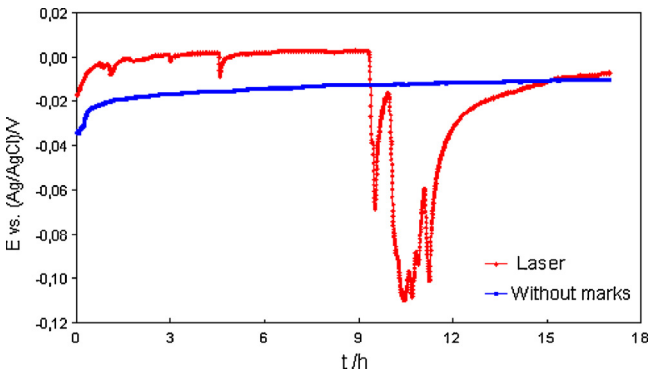

Fig. 3. OCP on laser marked and on blank ASTM F139 steel measured *versus* the exposure time in the PBS solution.

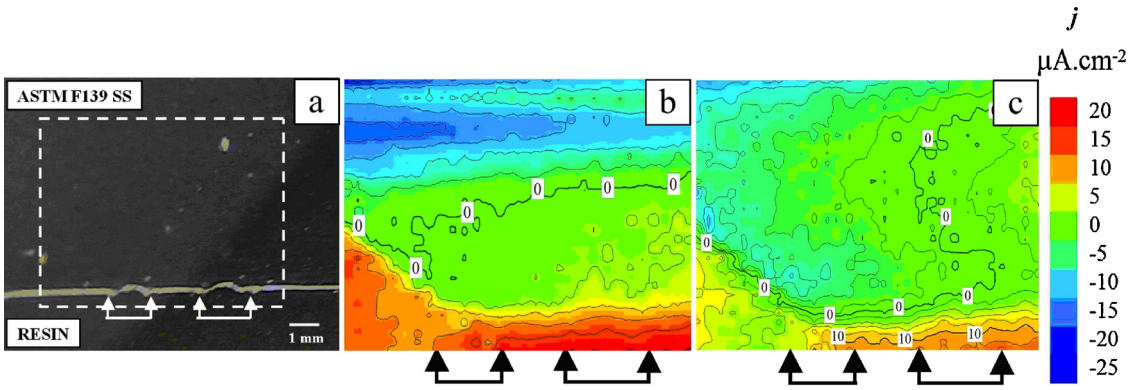

Fig. 4. (a) Optical microscopy image of a cross-section of laser marked ASTM F139 steel embedded in epoxy to simulate a crevice, (b) *i*-map measured after 20 min exposure in PBS solution and (c) after 40 min.

sequentially in PBS on the same area. Fig. 4a shows the cross-section of the surface with laser marks indicated by the white arrows. Fig. 4b shows the corresponding *i*-map measured after 20 min of exposure at OCP in PBS, where it can be seen, by the anodic currents around the arrows, that the onset of crevice corrosion is associated to the laser marks. After 40 min exposure (Fig. 4c) the associated current densities are lower but the crevice corrosion is still active.

To investigate if pitting nucleation is associated to the laser marks, SVET measurements were carried out under simultaneous polarization of the sample. Starting at $E = -435$ mV, the applied potential was increased in steps of 50 mV and an *i*-map measured at each step. Closer to the onset of pitting, *E* steps were decreased to 20 mV. At the starting potential, some anodic spots associated to the laser marks are already seen in Fig. 5a with local *i* values up to 50 μA/cm^2. The anodic spots are consumed and disappear during the experiment. Only at potentials close to E_{pit}, anodic spots with lower *i* values are again observed on the sample, mostly associated to the laser marks, as seen in Fig. 5b for $E = +610$ mV ($E_{AgCl/Ag}$). At a *E* value of +660 mV, a single pit is nucleated on the crossover of laser marks (Fig. 5c), on the measuring window, with local currents up to 1.4 mA/cm^2 right after the onset of pitting. Actually, other pits could also be observed on laser marks outside the SVET measuring window. Thus, the laser marks not only have very active spots well below E_{pit}, which are probably associated to metallic drops seen on the surface, but are also covered with a defective oxide layer, on which pits can more easily nucleate compared to the blank surface. During the test, the formation of stain on the metal surface under the solution, associated to anodic current (*i*), can be seen in real time (Fig. 5d), on the marked area. After the experiment has finished and the sample has been removed from the solution, some pits were identified by microscopy inspection on the same region (Fig. 5e).

The E_{pit} value for the laser marked ASTM F139 which ranged from 610 to 650 mV is in accordance with the value observed for AISI 316 L in 0.1 mol/L NaCl ($E_{pit} = 640$ mV *versus* $E_{AgCl/Ag}$) [19], but it is well below the value of its arc remelted, more resistant version ASTM F139 with $E_{pit} = 1162 \pm 80$ m. If the potential is directly set at +660 mV since the exposure starts, instead of slowly increasing it, as in CV or in 50 mV steps, as described above, then no strong differences are seen between laser marked and blank surfaces, and small pits nucleate randomly on the whole surface, not necessarily associated to the laser marks, as seen in Fig. 5f. It might be explained as it follows. When the potential is high enough, defective sites, associated or not to the laser marks, will dissolve anodically and remain active, leading to pits, differently to the behaviour observed at OCP.

XPS analysis results, prior to and after 10 min of argon ion etch, obtained on the laser marks and on the unmarked areas (blank surface) are shown in Table 1. It is clearly seen that the laser engraving process leads to large modification in the chemical composition of the surface. The oxide film chemical composition across the thickness was also strongly affected by the laser beam. At the laser affected areas, the outer layer is iron enriched and impoverished in Cr and Ni comparatively to the unmarked ones and it is even more evident at greater depths, as the comparison of the laser marked surfaces with the unmarked ones (blank) after 10 min of etch shows. This could be explained by Cr evaporation at the high temperatures generated by the laser engraving process and could partially elucidate the lower corrosion resistance of the laser marked surfaces.

The laser beam also had a significant influence on the electronic properties of the passive oxide film on the stainless steel surface, as the Mott–Schottky plots in Fig. 6 suggest for blank and laser marked surfaces. The flat band potential for the blank surface is approximately −450 mV ($E_{AgCl/Ag}$), which seems, if extrapolated from the p-type behaviour region, to be shifted to more positive potentials around −100 mV ($E_{AgCl/Ag}$). The details of the used Mott–Shottky procedure are described elsewhere [10]. Concerning the density of charge carriers, while the acceptors concentration is slightly affected by laser, decreasing from $4.84 \times 10^{+21}$ to $3.20 \times 10^{+21}$ carriers/cm^3, the donor concentration increases from $1.76 \times 10^{+21}$ to $9.92 \times 10^{+21}$ carriers/cm^3. Many authors have proposed that the different passive oxide layers formed on stainless steels exhibit variable semiconductor properties depending on the predominant defect present in the passive oxide film [16]. The passive film with a deficiency in metal ions or excess of cationic vacancies generally behaves as p-type, while n-type is developed in the passive films either by cationic transport through interstitial diffusion or by anion diffusion into the metal.

The donor charge concentration, associated with an n-type semiconductor is greater for the laser marked samples. This result indicates that a higher concentration of donors at the outer part of the oxide layer on the laser marks favours the incorporation of ions, such as chlorides, into the anions vacancies of the oxide film and its diffusion through it. This must favour the break down the oxide film and lead to pitting. The n-type semi-conductivity has been

Table 1
Weight ratios of ASTM F 139 stainless steel oxide layer measured by XPS on laser marked and blank surfaces.

Blank surface	Fe/(Fe + Cr + Ni)	Cr/(Fe + Cr + Ni)	Ni/(Fe + Cr + Ni)
Prior to etch	0.27	0.54	0.19
After 10 min etch	0.33	0.59	0.09
Laser marked	Fe/(Fe + Cr + Ni)	Cr/(Fe + Cr + Ni)	Ni/(Fe + Cr + Ni)
Prior to etch	0.57	0.32	0.11
After 10 min etch	0.72	0.14	0.13

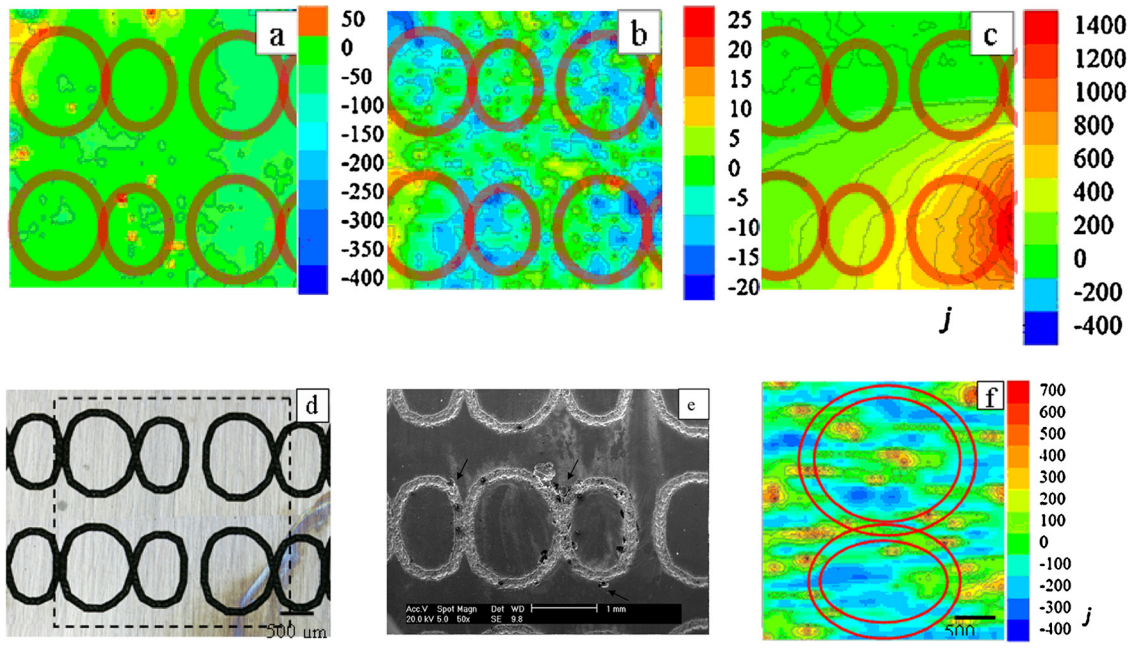

Fig. 5. (a) *i*-Map measured immediately after exposure of ASTM F139SS in PBS at an applied potential of $E = -435$ mV ($E_{AgCl/Ag}$), (b) *i*-map measured after increasing *E* stepwise in PBS from −435 mV up to $E = 610$ mV, (c) *i*-map measured after increasing *E* stepwise in PBS from −435 mV up to $E = 660$ mV and the onset of pitting, (d) View of the pitted surface under the solution according to (c) during the measurement just after pit nucleation, (e) SEM of pit after the experiment and (f) *i*-map measured when E is set at 660 mV immediately after exposure in PBS.

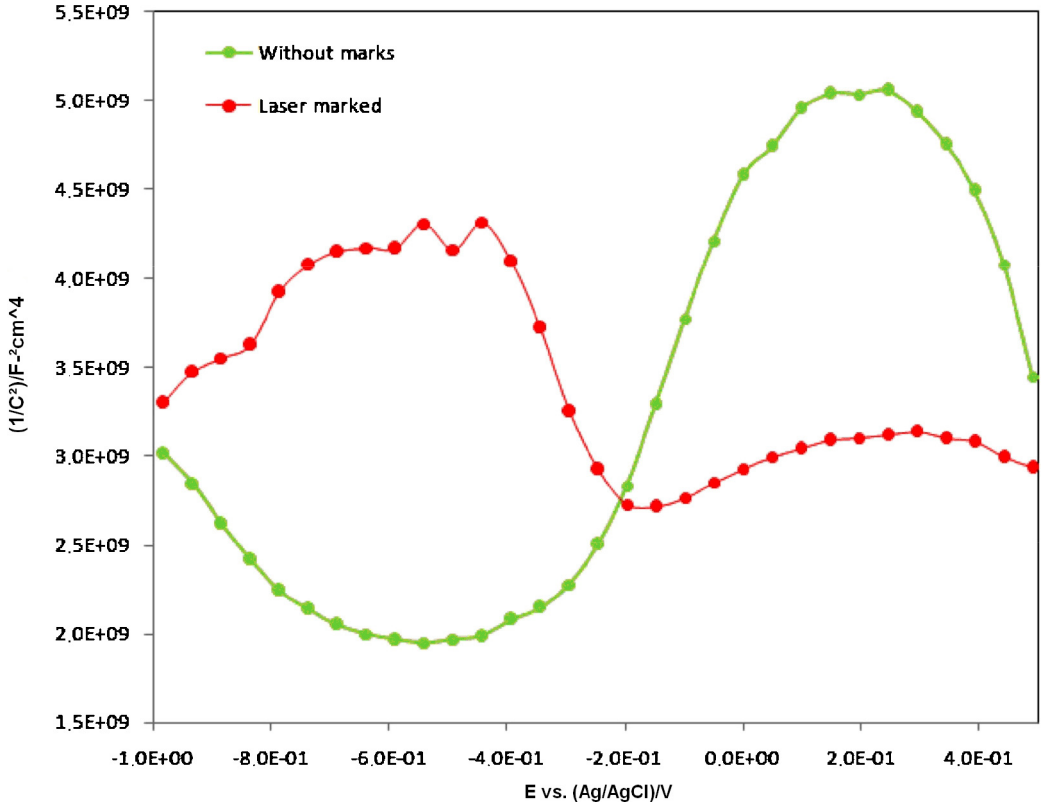

Fig. 6. Mott–Schottky plots for unmarked and laser marked ASTM F139 stainless steel samples measured in PBS.

correlated with the outer layer of the oxide, which is impoverished in nickel and in chromium [9–11,20].

4. Conclusions

Laser engraving of austenitic stainless steels produces highly defective surfaces that at OCP behave as anodic spots dissolving actively in phosphate buffered saline (PBS) and also favouring the nucleation of crevice corrosion. At higher potentials just below 660 mV ($E_{AgCl/Ag}$) the laser affected regions suffer pitting attack, more clearly when the applied potential is slowly increased stepwise from lower potentials.

The anodic spots that nucleate crevice and pitting corrosion are associated to the melting and rapid solidification of the metal surface by the laser marking, especially where the laser impinges twice on crossovers of the marking. XPS analysis indicates that the oxide on the affected surfaces is remarkably Ni-depleted. On the other hand, measurements of the capacitance of the metal surface shows that density of electron donor defects of the passive oxide increases from $1.76 \times 10^{+21}$ to *circa* $1 \times 10^{+22}$ charge carriers/cm^3 due to the laser incidence. The more defective outer part of the oxide layer favours ionic transport through the film, facilitating the film breakdown and leading to pitting corrosion. These two facts are believed to explain the increased corrosion susceptibility of the laser-marked stainless steel.

Acknowledgements

The authors acknowledge the Instituto de Ortopedia e Traumatologia of the Hospital das Clínicas da Faculdade de Medicina da Universidade de São Paulo and Baumer Ltda. for providing the material for this study. The authors also acknowledge Sabrina Neves da Silva from Eletrocorr-UFRGS for helping by SVET measurements.

References

[1] D.J. Lyman, W.J. Seare Jr., Biomedical materials in surgery, Mater. Sci. 4 (1974) 415.
[2] H. Amar, V. Vignal, H. Krawiec, C. Josse, P. Peyre, S.N. da Silva, L.F. Dick, Influence of the microstructure and laser shock processing (LSP) on the corrosion behaviour of the AA2050-T8 aluminium alloy, Corros. Sci. 53 (2011) 3215.
[3] R.A. Gittens, R. Olivares-Navarrete, R. Tannenbaum, B.D. Boyan, Z. Schwartz, Electrical implications of corrosion for osseointegration of titanium implants, J. Dent. Res. 90 (2011) 1389.
[4] B. Vuillemin, X. Philippe, R. Oltra, V. Vignal, L. Coudreuse, L.C. Dufour, E. Finot, SVET, AFM and AES study of pitting corrosion initiated on MnS inclusions by microinjection, Corros. Sci. 45 (2003) 1143.
[5] S.V. Lamaka, O.V. Karavai, A.C. Bastos, M.L. Zheludkevich, M.G.S. Ferreira, Monitoring local spatial distribution of Mg^{2+}, pH and ionic currents, Electrochem. Commun. 10 (2008) 259.
[6] H.S. Isaacs, The measurement of the galvanic corrosion of soldered copper using the scanning vibrating electrode technique, Corros. Sci. 28 (1988) 547.
[7] S. Kallip, A.C. Bastos, M.L. Zheludkevich, M.G.S. Ferreira, A multi-electrode cell for high-throughput SVET screening of corrosion inhibitors, Corros. Sci. 52 (2010) 3146.
[8] S. Kallip, A.C. Bastos, K.A. Yasakau, M.L. Zheludkevich, M.G.S. Ferreira, Electrochem. Commun. 20 (2012) 101.
[9] M. Da Cunha Belo, N.E. Hakiki, M.G.S. Ferreira, Semiconducting properties of passive films formed on nickel-base alloys type Alloy 600: influence of the alloying elements, Electrochim. Acta 44 (1999) 2473.
[10] L.V. Taveira, M.F. Montemor, M. Da Cunha Belo, M.G. Ferreira, L.F.P. Dick, Influence of incorporated Mo and Nb on the Mott–Schottky behaviour of anodic films formed on AISI 304L, Corros. Sci. 52 (2010) 2813.
[11] N.E. Hakiki, S. Boudin, B. Rondot, M. Da Cunha Belo, The electronic structure of passive films formed on stainless steels, Corros. Sci. 37 (1995) 1809.
[12] N.E. Hakiki, M. Da Cunha Belo, A.M.P. Simões, M.G.S. Ferreira, Semiconducting properties of passive films formed on stainless steels, J. Electrochem. Soc. 145 (1998) 3821.
[13] P. Schmuki, H. Böhni, J.A. Bardwell, In situ characterization of anodic silicon oxide films by AC impedance measurements, J. Electrochem. Soc. 142 (1995) 1705.
[14] J.F. Moulder, W.F. Stickle, P.E. Sobol, K.D. Bomben, in: J. Chastain (Ed.), Handbook of X-ray Photoelectron Spectroscopy, PerkinElmer Corporation, Physical Electronics Division, Eden Prairie, MN, USA, 1992.
[15] P.A.P. Nascente, Materials characterization by X-ray photoelectron spectroscopy, J. Mol. Catal. A: Chem. 228 (2005) 145.
[16] S. Ningshen, U. Kamachi Mudali, V.K. Mittal, et al., Semiconducting and passive film properties of nitrogen-containing type 316LN stainless steels, Corros. Sci. 49 (2007) 481.
[17] A. Shahryari, S. Omanovic, J.A. Szpunar, Electrochemical formation of highly pitting resistant passive films on a biomedical grade 316L stainless steel surface, Mater. Sci. Eng. C 28 (2008) 94.
[18] Z. Feng, X. Cheng, C. Dong, L. Xu, X. Li, Passivity of 316L stainless steel in borate buffer solution studied by Mott–Schottky analysis, atomic absorption spectrometry and X-ray photoelectron spectroscopy, Corros. Sci. 52 (2010) 3646.
[19] L.V. Taveira, G. Frank, H.P. Strunk, L.F.P. Dick, The influence of surface treatments in hot acid solutions on the corrosion resistance and oxide structure of stainless steels, Corros. Sci. 47 (2005) 757.
[20] N.E. Hakiki, M.F. Montemor, M.G.S. Ferreira, M. Da Cunha Belo, Semiconducting properties of thermally grown oxide films on AISI 304 stainless steel, Corros. Sci. 42 (2000) 687.